

Arresting the collapse of a catenary arch

Jemal Guven^{1,*} and Gregorio Manrique^{1,†}

¹*Instituto de Ciencias Nucleares, Universidad Nacional Autónoma de México, 04510 Ciudad de México, MEXICO*

It is well known that viable architectural structures can be identified by locating the critical points of the gravitational potential energy congruent with some fixed surface metric. This is because, if the walls are thin, the lowest energy modes of deformation are strain-free, and thus described by surface isometries. If it is to stand, however, an arch had better possess some minimum rigidity. The bending energy consistent with this construction protocol, we will show, can only depend on curvature deviations away from the reference equilibrium form. The question of stability, like the determination of equilibrium, turns on the geometry. We show how to construct the self-adjoint operator controlling the response to deformations consistent with isometry. As illustration, we reassess the stability of a simple catenary arch in terms of the behavior of the ground state of this operator. The energy of this state increases monotonically with the bending rigidity and it is possible to identify the critical rigidity above which the arch is rendered stable. While this dependence may be monotonic, it exhibits a number of subcritical kinks indicating significant qualitative changes in the ground state associated with eigenvalue crossovers among the unstable modes in the spectrum; the number of such competing modes increasing rapidly as the rigidity is lowered. The initial collapse of a subcritical arch is controlled by the ground state; on the critical threshold, there are two unstable modes of equal energy, one raising the arch at its center, the other lowering it. The latter dominates as the instability grows. The qualitative behavior of the ground state changes as the rigidity is lowered—its nodal pattern as well as its parity undergoing abrupt changes as the intervals between crossovers converge—complicating the prediction of the dominant initial mode of collapse.

I. INTRODUCTION

The first people to build with adobe, brick or stone would have been quick to appreciate that these materials tend to withstand compression considerably better than they do tension [1]. Unreinforced masonry will resist substantial compressive forces due to gravity before it crumbles; it will, however, develop cracks when subjected to even modest tension. But, before it fails, it will behave—to a surprisingly good approximation—as an inextensible medium: it neither stretches nor shrinks.

Contemporary building materials, we know, are not limited by tension like masonry, and they will buckle rather than crumble. Nevertheless, the most relevant modes of deformation consistent with the integrity of any thin-walled free-standing structure, whether it be a cathedral vault or the canopy of an airport terminal, are the same as those that constrain the design of masonry. For, if the walls are thin compared to their radius of curvature, the modes costing the least energy are those preserving distances along

the surface of the wall. In mathematical terms, this means that they leave the metric on this surface fixed: they are isometries. The subject of isometry was discussed with (unusual) relish in volume five of Spivak [2]. The curious reader will find complementary treatments in references [3–5] and, perhaps most comprehensively, in Steven Verpoort’s thesis [6]. Not only are the relevant degrees of freedom geometrical, so also are the constraints connecting them. Despite the difference in scale, in this sense, the walls of any building—viewed in the large—are no different from a folded thin sheet, be it graphene or a modest A4 sheet of paper. The latter has come under increasing scrutiny in recent years not only for its technological importance but also as a legitimate problem—not to be underestimated—falling within the scope of soft matter [7]; for a sampling of the rapidly expanding literature see, for example, [8–11]. Technically, even the parametrization of an isometrically folded thin sheet, never mind the physics, poses its own challenges (as emphasised forcefully in a recent paper [12]). In retrospect, the neglect of isometry by physicists or engineers until the closing years of the twentieth century will require some explanation.

* *E-mail address:* jemal@nucleares.unam.mx

† *E-mail address:* gregorio.manrique@correo.nucleares.unam.mx

We will argue that, despite the differences in the underlying physics and the disparity in scale involved, the geometrical framework used to describe thin sheets can be tweaked to shed interesting light on the behavior of contemporary building materials and, whenever the thin wall idealization is appropriate, the behavior of masonry itself. Paradoxical as it may seem, there is a limit in which it is not unrealistic to think of masonry as a soft material.

The recognition that a catenary somehow provides the optimal structure for spanning an opening predates Robert Hooke [13]. He was, however, the first to articulate why in the language of mechanics; indeed, the significance of his discovery impressed him sufficiently that he squandered valuable time composing an anagram in Latin to record it [14–16]. Deciphered and translated, the well-known anagram declaims “*As hangs the chain, so but inverted stands the arch*”. A hanging rope of fixed length, suspended between two fixed points, will minimize its potential energy when it traces out a catenary; this part is an elementary exercise in the calculus of variations accommodating the local constraint on its length. Inverted, it will form an arch. In the process, the tension in the chain gets converted to compression and because the lines of thrust are tangent to the catenary they are steered safely into the foundations or lateral supports [17]. Curiously, in contrast to the law reluctant schoolchildren associate with Hooke, there is not a strain in sight.

More generally, if the gravitational potential energy is stationary with respect to deformations preserving the metric, the stress will be tangential and the surface viable. Remarkably, this is true irrespective of its specific material properties. The problem is completely geometrical. The equations leading to this conclusion can be derived by applying the calculus of variations using Lagrange multipliers to impose isometry as a constraint. We will show how to do this following the method developed by one of the authors (with Martin Müller) in another context [18].

Despite the simplicity of Hooke’s protocol, it remains the basis for identifying rather more complex optimal geometries, with custom-

designed software enlisted to implement it in its full two-dimensional glory. The extraordinary scope of the approach is illustrated in references [19] and [20]. Its aesthetic potential was, of course, anticipated by Antoni Gaudí, and more recently by the late Zaha Hadid [21, 22]. One could quibble over the occasionally awkward aesthetics—or question the impulses driving the construction of such cavernous structures—but such questions fall well outside the scope of this paper. There is, however, a crucial aspect of the protocol that is not addressed in the optimization process: an assessment of the stability of these structures in the geometrical spirit of the protocol [23]. This turns out not to be straightforward; and geometry plays an even more significant role than it does in the design itself.

The stress, of course, is not constant within an arch. In Hooke’s protocol, however, it depends only on the geometrical aspect ratio and its mass; it does not depend on any other material properties. Notably, resistance to bending is ignored—with impunity—in the design protocol; so it cannot contribute to the stress distributed within the equilibrium structure. This may be very well in a hanging rope but, in an arch, it cannot be the full story. For the protocol also ignores the fact that the gravitational potential energy is a maximum in a catenary arch. As such, it would collapse immediately, like a falling rope whether or not the one-third rule of thumb—confining the lines of thrust—is satisfied [24, 25]. Unlike a pencil, standing on its lead, the number of unstable modes of the arch consistent with isometry is infinite (or certainly large); the modes with the shortest wavelength turn out to be the most unstable gravitationally. While the cost to bend the arch may play no role in determining the equilibrium shape, or even contribute to the stress, it clearly does play a very important role in counteracting this instability.

But this begs the question: what is the appropriate bending energy? The energy consistent with Hooke’s protocol cannot be the familiar symmetric energy quadratic in curvature: for, if it were, the equilibrium would itself possess bending energy which would in turn shift the equilibrium, introducing additional bending

stresses within the structure. Hooke’s protocol would be rendered as good as useless. The appropriate bending energy can only penalize deviations away from the equilibrium *reference* state, at lowest order it will be quadratic in the deviation. There is no bending energy in the equilibrium state. This is not only true in the traditional construction of a masonry arch which involves the use of centring, removed when the cement has cured, but also in the assembly of pre-formed units in contemporary construction where the accommodation of tension is not an obstacle. Indeed, this understanding is implicit in a promotional video produced by Norman Foster and Partners, where the principle informing the design of an airport terminal is illustrated using a chain with resin sprayed onto the hanging chain to lend it the rigidity it needs to stand upon inversion [26, 27]. The bending energy possesses an inhomogeneous spontaneous curvature determined by the equilibrium we spray.

Bending energies with this property may vanish in the equilibrium state but will contribute at second and higher order in deformations about it. It is also manifestly positive. If sufficiently positive, the arch will stand.

For simplicity, we will suppose that a single parameter μ characterizes the bending rigidity of the medium. This simple energy is completely geometrical. Thus the question of stability, like the Hookean construction itself, is a geometrical question. Extensions to accommodate anisotropies or inhomogeneities are all straightforward in principle, but obscure the essential geometrical nature of the problem.

To examine stability under small deformations it is necessary to expand the total energy—gravitational potential plus bending energy—constrained by isometry, to quadratic order about the equilibrium structure. It is not obvious that the inclusion of the constraint at this order is going to be tractable analytically. By happy accident, we find it turns out to be. The key result of this paper is the identification of the self-adjoint linear operator controlling small deformations and thus the stability of the structure. Technically there is a snag: this operator is sixth-order in derivatives—a consequence of the

constraint; an order that one is not accustomed to chance upon in the description of physical systems.

To illustrate how our framework may be applied, we will examine a symmetric catenary arch and assess its stability from this point of view. This is as simple as it gets yet not quite as simple as we would have hoped. The compensation is that it turns out to be considerably more interesting than expected.

If the parameter μ is positive the spectrum of the operator is bounded from below. There is also a critical rigidity μ_c above which the lowest eigenvalue turns positive and the arch is rendered stable with respect to small deformations; below μ_c the arch will be unstable; its dominant mode of collapse described by the eigenfunction of this operator which corresponds to this lowest eigenvalue. To this point the behavior accords with intuition. The lowest eigenvalue also grows monotonically with μ . However, as it grows, it displays kinks, signalling interesting behavior where these occur.

It is useful to think of the self-adjoint operator as a Hamiltonian describing a quantum mechanical particle moving in one-dimension—albeit an unusual Hamiltonian sixth order in momentum—and to identify the eigenfunction which corresponds to the lowest eigenvalue as the ground state of this Hamiltonian.

When the arch is just subcritical, the ground state is symmetric and exhibits two nodes. This single state represents two physically distinct unstable modes: one raising the arch at its center, the other lowering it. This degeneracy cannot be resolved at quadratic order and it is necessary to proceed to the next order in deformations to identify which of the two is the more unstable. It turns out to be the mode lowering the arch at its center and this mode will dominate as the instability grows, consistent with observations. The hinge-points where failure occurs are located at the three anti-nodal positions along the arch. This interpretation of this feature appears to be new. We predict how the positions of these hinges depend on the aspect ratio as well as the rigidity.

The spatial behavior of the ground state de-

pends somewhat sensitively on how far below criticality the rigidity lies, indicating a qualitative change in the instability as the rigidity is reduced. Below a second critical value, located at the last kink, the unstable symmetric state with two nodes is replaced by an antisymmetric state with an additional node as the ground state. The ground state is no longer the state with the lowest number of nodes and it is no longer symmetric. As the rigidity is lowered even further, the number of nodes displayed by the ground state generally increases as one passes through the succession of discrete values of μ , where the kinks are located. The number of unstable states also increases. What is more, the number of nodes exhibited by these states does not correlate simply with their energy which, unlike the ground state energy, does not generally increase monotonically with μ . Predicting the mode of collapse is complicated accordingly. The collapse of a simple catenary arch, as simple an architectural structure as one can conceive, turns out to be an unexpectedly complex process.

It is possible that the reader may not be interested in this specific problem. However, the issues addressed here and their treatment are increasingly relevant in soft matter and the recently dubbed field of extreme mechanics where isometries play an important role in understanding both the morphology and the physical behavior of thin sheets, whether macroscopic or nanoscaled. The framework we introduce can be adapted to accommodate different bending energies as well as external forces.

II. GRAVITATIONAL POTENTIAL AND BENDING ENERGY

If the structure is thin compared to its radius of curvature, we can represent it as a parametrized surface in three-dimensional space, $(u^1, u^2) \mapsto \mathbf{X}(u^1, u^2)$. Here $\mathbf{X} = (X^1, X^2, X^3)$ is a triplet of functions, providing a Cartesian representation of the surface. The gravitational potential energy is given by

$$H_0[\mathbf{X}] = \rho \int dA h, \quad (1)$$

where $h = \mathbf{X} \cdot \mathbf{k}$ is the local height above a given horizontal plane, and \mathbf{k} is the normal to this plane. The measure of surface area dA is invariant under isometry. We will suppose for simplicity that the mass density ρ is uniform and absorb the acceleration due to gravity into its definition. The Hookean equilibria are critical points of H_0 within the class of geometries with fixed boundaries and a given induced metric. The latter is given by

$$g_{ab} = \mathbf{e}_a \cdot \mathbf{e}_b, \quad (2)$$

where $\mathbf{e}_a = \partial_a \mathbf{X}$, $a, b = 1, 2$ are the two surface tangent vectors adapted to the parametrization. We will examine the corresponding equilibria in Section III.

Equilibrium biased bending energy: The bending energy of a surface is quadratic in its curvature; if it is symmetric and isotropic, and the reference geometry is flat, it is given by (see, for example, [28])

$$H_{B0} = \frac{1}{2} \mu \int dA (C_1 + C_2)^2 + \bar{\mu} \int dA C_1 C_2. \quad (3)$$

Here C_1 and C_2 are the principal curvatures, namely, the two real eigenvalues of the extrinsic curvature tensor, a measure of how fast the surface normal \mathbf{n} rotates into one direction as one moves it along another,

$$K_{ab} = \mathbf{e}_a \cdot \partial_b \mathbf{n}. \quad (4)$$

The Gaussian curvature $C_1 C_2$ is an isometry invariant. Modulo the two material parameters, μ and $\bar{\mu}$, this energy depends only on the geometry. If sufficiently thin (of thickness t), we also know that the surface will bend before it stretches [29]: this is because the bending energy scales as t^3 , whereas stretching energy increases linearly with t . We will comment on potential limitations of this approximation in the conclusions.

In the Hookean construction, the appropriate bending energy, H_B , cannot play any role in determining the equilibrium nor in determining the distribution of stress. As such, both H_B and its first variation, δH_B , must vanish in equilibrium. Neither condition is satisfied by H_{B0} . Nor

is the reference geometry flat. The simplest energy consistent with these criteria is given by

$$H_B = \frac{1}{2} \mu \int dA \sum_I (\mathcal{C}_I - \mathcal{C}_I(u))^2, \quad (5)$$

where $\mathcal{C}_1[u]$ and $\mathcal{C}_2[u]$ are the curvatures of the undeformed reference geometry, the equilibrium determined by the minimization of the gravitational potential energy consistent with the constraints. Because we are only interested in isometries there is no need to introduce a term analogous to the second term, proportional to $\bar{\mu}$, appearing in Eq.(3).

The two curvatures $\mathcal{C}_1[u]$ and $\mathcal{C}_2[u]$ appear to play the role of anisotropic, position dependent, spontaneous curvatures. However, it would be wrong to think of them as independent parameters in the model, determined as they are by the equilibrium we are deforming. Constant isotropic spontaneous curvatures are familiar in membrane biophysics where they are introduced to explain the global morphology of cellular membranes [30, 31]; they can also arise due to the differences in the area of the two sides of a membrane bilayer [32], or indeed a difference in the areas of the two bilayers within a lamellar tetralayer enclosing a lumen, as conjectured in [33]. Energies involving constant anisotropic spontaneous curvatures occur in two-dimensional liquid crystals; curved nematics on a fluid membrane substrate may imprint their curvature on that substrate [34, 35]. Spatially varying anisotropic target curvatures are also relevant in the modelling of the controlled lateral swelling of thin elastic sheets [36]. What distinguishes the energy (5) from these is the fact that $\mathcal{C}_1[u]$ and $\mathcal{C}_2[u]$ are themselves undetermined until the Hookean optimization is completed. This is a very important feature of the model [37]. While H_B vanishes in equilibrium, it does contribute at second and higher order in departures away from equilibrium. It is positive and thus tends to stabilize the geometry. There are two questions we wish to answer: how large must μ be to achieve this? What is the nature of the instability if μ falls short? As we have hinted, and as we will show, the answer to the latter question presents a number of surprises.

III. HOOKE'S SHAPE EQUATIONS

The critical points of the energy can be identified by using the method of Lagrange multipliers to impose the isometry constraint. To solve the Hookean problem, one introduces the constrained functional (the metric is defined in terms of \mathbf{X} by Eq.(2) and $g_{ab}^{(0)}(u^1, u^2)$ is a fixed metric of our choosing),

$$H_{0C}[\mathbf{X}, \sigma^{ab}] = \rho \int dA h - \frac{1}{2} \int dA \sigma^{ab} (g_{ab} - g_{ab}^{(0)}). \quad (6)$$

A familiar analogue is the treatment of vector fields with a fixed—usually vanishing—divergence. To determine the Euler-Lagrange equations, we examine how the energy responds to a surface deformation $\mathbf{X}(u^1, u^2) \rightarrow \mathbf{X}(u^1, u^2) + \delta\mathbf{X}(u^1, u^2)$. The presence of the local multipliers $\sigma^{ab}(u^1, u^2)$ frees us to treat the three Cartesian deformations, $\delta\mathbf{X}$, independently, unconstrained by isometry [18].

Qualitatively, normal and tangential deformations are very different. As such, it is useful to decompose the deformation explicitly along the respective directions:

$$\delta\mathbf{X} = \Psi^a \mathbf{e}_a + \Phi \mathbf{n}. \quad (7)$$

The normal and tangent Euler-Lagrange equations are identified using methods developed elsewhere (we use [18, 38]):

$$(\sigma^{ab} - \rho h g^{ab}) K_{ab} = \rho (\mathbf{n} \cdot \mathbf{k}); \quad (8a)$$

$$\nabla_a \sigma^{ab} = 0. \quad (8b)$$

Here ∇_a is the covariant derivative compatible with g_{ab} ; the normal equation involves the extrinsic curvature K_{ab} defined in Eq. (4). In general, Eqs.(8) would underdetermine the geometry if g_{ab} were not fixed. The element of freedom in the design process is captured mathematically by the choice of metric. Eqs.(8) are, themselves, well-known. They appear in references [19] and [20]. While neither derivation involves the calculus of variations this is, however, the obvious approach if one is to proceed and assess the stability of the equilibrium geometry.

Whereas the stress associated with the constraint is conserved, the total stress

$T^{ab} = \sigma^{ab} - \rho h g^{ab}$, adding the contribution from gravity, is not: $\nabla_a T^{ab} = -\rho(\mathbf{e}^b \cdot \mathbf{k})$. It is the total stress, however, that needs to be consistent with the properties of the medium; in masonry, it must be compressive everywhere (or approximately so); equivalently, T^{ab} must be positive definite.

Symmetric catenary vault: As a prelude to the assessment of its stability, we re-examine briefly—in this approach—a cylindrical vault described in an adapted Cartesian parametrization, (X, Y) , by $h = h(X)$. This is not, of course, the most straightforward approach if one is only interested in equilibrium. Indeed, an elementary, if incomplete, derivation using force balance is provided at the beginning of Gray's graphic introduction to differential geometry [40].

Eq.(8b) implies that $\sigma_{XX} = \sigma_0$, a constant; whereas $\sigma_{YY} = 0$. Using the identification of K with the Frenet curvature along the curve described by h , $\kappa = -\ddot{h}/(1 + \dot{h}^2)^{3/2}$, where dot denotes d/dX , Eq.(8a) integrates to yield a quadrature $\dot{h}^2 - C^2 \tilde{h}^2 = -1$, where we define $\tilde{h} := h - \sigma_0/\rho$. This possesses the familiar solution: $\tilde{h} = C^{-1} \cosh CX$. The two unknown constants C and σ_0 are determined by the boundary conditions. For a cross-section of maximum height H , and width $2L$, one determines σ_0 implicitly as a function of the aspect ratio:

$$\sigma_0/\rho = (\sigma_0/\rho - H) \cosh(L/[\sigma_0/\rho - H]). \quad (9)$$

This relationship is represented in Fig. 1. It is now straightforward to read off the compressive stress at any position along the arch.

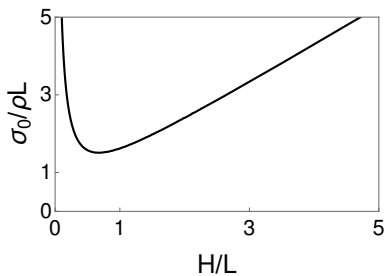


FIG. 1: The stress associated with the isometry constraint as a function of the aspect ratio in a catenary arch. σ_0 is positive;

in addition, $\sigma_0/\rho > H$ so that the total stress $T_0 = \sigma_0 - \rho h > 0$ is compressive everywhere.

IV. SECOND VARIATIONS

We now turn to the question of stability of the equilibrium structure. This involves expanding the total energy, the sum of the potential energy (1) and bending energy (5) to second order in deformations about this structure. Again these deformations need to be consistent with isometry. We will do this in general, for fixed boundaries. The correct boundary conditions on free boundaries is a vexed issue that will be addressed elsewhere.

(1) *Potential energy* One can show that the second variation of the constrained potential energy is given by (we abuse notation by writing H_0 instead of H_{0C}) $\delta^2 H_0 = -\int dA T^{ab} \nabla_a \delta \mathbf{X} \cdot \nabla_b \delta \mathbf{X}$. Because the total stress T^{ab} is positive in compression, it follows that $\delta^2 H_0 < 0$. The deformation $\delta \mathbf{X}$ appearing here is constrained by isometry, or equivalently, at this order: $\mathbf{e}_a \cdot \nabla_b \delta \mathbf{X} + \mathbf{e}_b \cdot \nabla_a \delta \mathbf{X} = 0$. This constraint can be recast at linear order in terms of the projections of $\delta \mathbf{X}$ (7) as

$$\nabla_a \Psi_b + \nabla_b \Psi_a + 2K_{ab} \Phi = 0. \quad (10)$$

This allows $\delta^2 H_0$ to be rewritten

$$\delta^2 H_0 = -\int dA T^{ab} [A_a A_b + \frac{1}{4} g_{ab} (\nabla \times \Psi)^2], \quad (11)$$

where we introduce the surface vector field

$$A^a := \nabla^a \Phi - K^{ab} \Psi_b, \quad (12)$$

and define $\nabla \times \Psi = \epsilon^{ab} \nabla_a \Psi_b$ using the anti-symmetric Levi-Civita tensor ϵ^{ab} . Each of the two terms appearing in Eq.(11) is manifestly negative.

(2) *Bending energy* If $\delta \mathbf{X}$ is an isometry, the second variation of the equilibrium biased bending energy (5) is given by

$$\delta^2 H_B = \mu \int dA \sum_I (\delta C_I)^2, \quad (13)$$

where δC_I is the deformation induced in the curvature C_I under the isometry. We now use the trivial algebraic identity $2C_1C_2 = (C_1 + C_2)^2 - C_1^2 - C_2^2$ to express the Gaussian curvature as a difference. As a consequence, under isometry, $\sum_I(\delta C_I^2) = (\sum_I \delta C_I)^2$. But $\sum_I C_I = g^{ab}K_{ab}$. Thus

$$\delta^2 H_B = \mu \int dA (\delta K)^2. \quad (14)$$

Remarkably, it is only necessary to determine the deformed trace to evaluate the second variation of the bending energy. This can be shown to be given, for an isometry, by $\delta K = -\nabla_a(\nabla^a\Phi - K^{ab}\Psi_b) = -\nabla_a A^a$, where A^a defined in Eq.(12) appears once again. This follows from the general expression $\delta K = -(\nabla^2 + K^{ab}K_{ab})\Phi + \Psi^a \partial_a K$ (see, for example, [38]), and the isometry constraint, Eq. (10).

One can now add the two contributions to identify the total second variation, $\delta^2 H_{\text{total}} = \delta^2 H_B + \delta^2 H_0$. This expression is general. Indeed, we do not need to be interested specifically in gravity. Our analysis continues to be valid with an obvious modification if gravity is replaced by a more general external force derivable from a potential V , with the replacement h , linear in \mathbf{X} , by $V(\mathbf{X})$.

We are specifically interested in the critical value of the rigidity μ above which $\delta^2 H_{\text{total}} > 0$. We will show how to determine this value for a symmetric catenary arch.

V. STABILITY OF THE CATENARY ARCH

We first examine deformations preserving the cylindrical symmetry. The second variation now simplifies to give

$$\delta^2 H_{\text{total}} = \int ds [\mu A'^2 - (\sigma_0 - \rho h)A^2], \quad (15)$$

where $A = \Phi' - \kappa\Psi$ is now a scalar, and again κ is the Frenet curvature of the catenary. Ψ is the projection of $\delta\mathbf{X}$ along the unit tangent, Φ again is the normal deformation, and prime indicates a derivative with respect to arc-length. The two fields Φ and Ψ are not independent, constrained as they are by the cylindrical reduction

of Eq.(10): $\Psi' + \kappa\Phi = 0$. Note that the second term appearing in Eq.(11) does not contribute. It does, however, contribute if the deformation is not cylindrical, but curls will also contribute to the bending energy so, a non-vanishing curl, does not necessarily imply that a higher rigidity is required to establish stability.

The natural way to proceed might appear to be to eliminate Ψ in favor of Φ , as done in [41]. After all, intuitively, one tends to think of the tangential deformations as tagging their normal counterparts, not the other way around. The fixed boundary conditions, however, obstruct this course. Counterintuitive as it may seem, they do permit Φ to be eliminated in favor of Ψ' and this can be done globally because $\kappa > 0$. We now can express the scalar A in terms of Ψ : $A = \mathcal{F}\Psi$, where the differential operator \mathcal{F} is given by

$$\mathcal{F} := -\partial_s \frac{1}{\kappa} \partial_s - \kappa. \quad (16)$$

Because the boundary is fixed, $\Psi = 0$, $\Psi' = 0$, and $\Psi'' = 0$ there. One can now integrate by parts to rewrite

$$\delta^2 H_{\text{total}} = \int ds \Psi \mathcal{H}_\mu \Psi, \quad (17)$$

where \mathcal{H}_μ is self-adjoint on the appropriate Hilbert space of functions. This operator is the sum of a positive definite sixth-order operator \mathcal{H}_1 associated with bending energy and a negative definite fourth-order \mathcal{H}_0 associated with the gravitational potential:

$$\mathcal{H}_\mu = \mu\mathcal{H}_1 + \mathcal{H}_0; \quad (18)$$

where

$$\mathcal{H}_1 = -\mathcal{F} \partial_s^2 \mathcal{F}; \quad (19a)$$

$$\mathcal{H}_0 = -\mathcal{F}(\sigma_0 - \rho h)\mathcal{F}. \quad (19b)$$

Each of the two operators is a manifestly self-adjoint operator sandwich formed by the operator \mathcal{F} , itself self-adjoint, defined by Eq.(16).

To borrow the language of quantum mechanics, the second variation $\delta^2 H_{\text{total}}$ can be thought of as the *expectation value* of the operator \mathcal{H}_μ (the quantum mechanical *Hamiltonian*) in the

(normalized) state Ψ . In this spirit, we adopt the Dirac shorthand [42]

$$\delta^2 H_{\text{total}}[\mathbf{X}] = \langle \Psi | \mathcal{H}_\mu | \Psi \rangle. \quad (20)$$

Identifying the spectrum of \mathcal{H}_μ : The operator \mathcal{H}_μ possesses a discrete spectrum: $\mathcal{H}_\mu |\lambda_{\mu,n}^\pm\rangle = \lambda_{\mu,n}^\pm |\lambda_{\mu,n}^\pm\rangle$, $n = 1, 2, 3, \dots$; because \mathcal{H}_μ is self-adjoint its eigenvalues $\lambda_{\mu,n}^\pm$ are real and the eigenstates (or modes) $|\lambda_{\mu,n}^\pm\rangle$ corresponding to distinct eigenvalues are orthogonal. We also know that each eigenstate possesses a definite parity, indicated $+(-)$ if even (odd). This is because \mathcal{H}_μ is even under reflection in the origin, sending $s \rightarrow -s$, or equivalently, the operator Π representing the reflection commutes with \mathcal{H}_μ ; as a consequence $\Pi |\lambda_{\mu,n}^\pm\rangle = \pm |\lambda_{\mu,n}^\pm\rangle$. Notice that the isometry constraint $\Psi' + \kappa\Phi = 0$ implies that Ψ is odd whenever Φ is even.

We order the $|\lambda_{\mu,n}^\pm\rangle$ by the number of nodes, n . Thus $|\lambda_{\mu,1}^-\rangle$ represents an odd tangential mode with one node (its normal counterpart will be even with two nodes); $|\lambda_{\mu,1}^+\rangle$ represents an even tangential mode with two nodes, and so on. Even and odd parity states are orthogonal: $\langle \lambda_{\mu,n}^+ | \lambda_{\mu,m}^- \rangle = 0$ for any n and m . In general, this ordering differs from the ordering by energy ($\lambda_{\mu,n}^\pm$), but when μ is very large (very small) the two orderings do correspond (anti-correspond).

One does not expect to find a simple analytical expression for the eigenstates or even the spectrum of \mathcal{H}_μ . It is possible to perform back-of-the-envelope approximations when the number of nodes is large and we will do this. In general, however, Rayleigh-Schrödinger perturbation theory is least useful where the physics is most interesting and one needs to develop a numerical approximation. To do this, we expand the tangential state $|\Psi\rangle$ with respect to an appropriate complete orthonormal basis $\{|\Psi_n^\pm\rangle, n = 1, 2, 3, \dots\}$ that is consistent with the boundary conditions as well as possessing a definite parity [43]:

$$|\Psi\rangle = \sum_{n=1,\pm}^{\infty} C_n^\pm |\Psi_n^\pm\rangle. \quad (21)$$

These states are not themselves eigenstates of \mathcal{H}_μ . If we now expand the right hand side of Eq.(20) with respect to the $\{|\Psi_n^\pm\rangle\}$, we find

$$\langle \Psi | \mathcal{H}_\mu | \Psi \rangle = \sum_{n,m,\pm} C_n^\pm C_m^\pm B_{nm}^\pm, \quad (22)$$

where

$$B_{nm}^\pm = \langle \Psi_m^\pm | \mathcal{H}_\mu | \Psi_n^\pm \rangle. \quad (23)$$

The matrix elements connecting even and odd states vanish because of the parity of \mathcal{H}_μ and the definite parity of the basis elements: $\langle \Psi_m^\pm | \mathcal{H}_\mu | \Psi_n^\mp \rangle = 0$. Our task is reduced to the diagonalization of two square matrices, B_{mn}^+ and B_{mn}^- . This identifies the eigenvalues $\lambda_{\mu,n}^\pm$ as well as the corresponding eigenstates.

The ground state energy: For each $\mu > 0$, the operator \mathcal{H}_μ possesses a lowest eigenvalue E_μ ; the corresponding eigenstate is the analog of the quantum mechanical ground state, which we label, $|0_\mu\rangle$: $\mathcal{H}_\mu |0_\mu\rangle = E_\mu |0_\mu\rangle$. The second variation (20) is bounded from below by E_μ : $E_\mu \leq \langle \Psi | \mathcal{H}_\mu | \Psi \rangle$ for all normalized $|\Psi\rangle$.

We are interested in the functional dependence of E_μ on μ . It is straightforward to show that E_μ increases monotonically with μ : if $\mu_1 > \mu_2$, then

$$\langle \Psi | \mathcal{H}_{\mu_1} | \Psi \rangle - \langle \Psi | \mathcal{H}_{\mu_2} | \Psi \rangle = (\mu_1 - \mu_2) \langle \Psi | \mathcal{H}_1 | \Psi \rangle > 0. \quad (24)$$

We are specifically interested in identifying the critical value μ_c , above which E_μ turns positive, signalling the transition from instability to stability. Once it turns positive the inequality (24) ensures that it remain positive. We now apply the numerical approximation sketched earlier to identify E_μ . Significantly, it is not a linear function of μ . As we will see, it is not even a smooth function of μ . Above μ_c , however, the value of E_μ is controlled by \mathcal{H}_1 . This implies that, asymptotically, E_μ does depend linearly on μ , consistent with our expectations.

The numerically determined E_μ is plotted as a function of μ for a representative aspect ratio in Fig. 2.

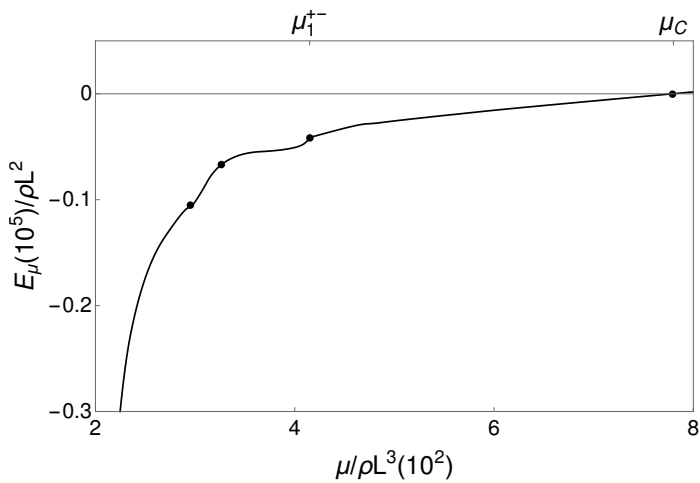


FIG. 2: Ground state energy E_μ as a function of μ for $H/L = 1/5$. It increases monotonically with μ , vanishing at the dimensionless critical value $\mu_c = 7.9$ above which the arch is stable with respect to small deformations. This will be seen to occur at the value of μ (μ_1^-) where the (non-monotonic) eigenvalue $\lambda_{\mu,1}^-$ changes sign for the last time. An infinite sequence of subcritical kinks is observed in the behavior of E_μ . The last three of these are indicated explicitly in the figure. The final kink occurs when $\mu/\rho L^3(10^2) = \mu_1^{+-} = 4.2$, where $\lambda_{\mu,1}^-$ and $\lambda_{\mu,1}^+$ crossover for the (last) time. The origin of these kinks will be discussed in the text.

Critical Rigidity and the aspect ratio: The dependence of μ_c on the aspect ratio, H/L is presented in Fig. 3. Its behavior correlates qualitatively with that of the constraining stress. We have compared these predictions with the results of a simple experiment involving a thin plastic sheet suspended between two fixed walls a variable distance apart, $2L$. The initial catenary sheet collapses under inversion. A resin lending rigidity to the sheet is now applied uniformly and the weight (a measure of μ) recorded. This is repeated a number of times for each L until such point that the sheet does not collapse when inverted. The results agree qualitatively with our numerical prediction.

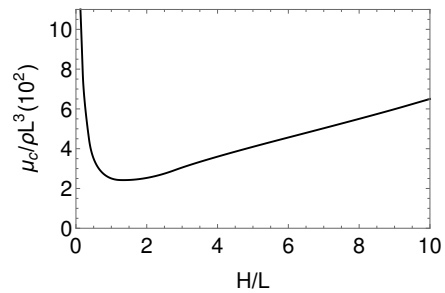


FIG. 3: Critical Rigidity as a function of the aspect ratio.

In a subcritical arch, the eigenstate $|\lambda_{\mu,n}^\pm\rangle$ that is assuming the role of ground state, $|0_\mu\rangle$ does not possess a fixed number of nodes as μ is varied, nor is its parity fixed. Because this state controls the instability of the catenary, the nature of this instability itself depends qualitatively on the value of μ . As we will see, the kinks appearing in Fig. 2 indicate the locations where these transitions occur. To understand this behavior, it is necessary to study in some detail the dependence of the unstable eigenstates of \mathcal{H}_μ on μ .

As μ is decreased below μ_c , the number of negative eigenvalues—corresponding to unstable modes—typically increases. Let us first look at small values of μ . In the limit of a fictitious catenary rope with no bending energy, the ground state energy in the continuum limit will be unbounded from below, corresponding to a state with an infinite number of nodes. In practice, however, there will be a short distance cutoff, so that the corresponding state is the one with the maximum number of nodes consistent with this cutoff (n_{\max}).

Short wavelength modes: Suppose that the wavelength is small, or equivalently $n \gg \kappa L$, and that H/L is small so that h/L can be treated as slowly varying and the curvature κ is approximately constant. In this regime, $\mathcal{H}_0 \approx -C_0 \partial_s^4$, where C_0 is a constant. As bending energy is dialed in, it will penalize the high curvatures in these short wavelength modes. In the same approximation, $\mathcal{H}_1 \approx -\mu C_1 \partial_s^6$, where C_1 is another constant. The operators \mathcal{H}_0 and \mathcal{H}_1 effectively commute in this regime. The eigenstates of \mathcal{H}_μ can be expanded in

trigonometric functions, with corresponding eigenvalues, $\lambda_{\mu n} \approx C_1 n^4 (\mu n^2 - C_0/C_1)$, where a fixed geometrical factor has been absorbed into the definition of the constants. Note that, while the trigonometric functions themselves are not consistent with the boundary conditions, the error can be ignored when n is large. In this regime, even and odd modes become energetically degenerate. The eigenvalues increase linearly with μ in this regime. This is not true in general: not only do they not increase linearly, they do not even behave monotonically, the monotonic behavior of the ground state notwithstanding.

If $\mu = 0$, $\lambda_{\mu n} \approx -C_0 n^4$. One sees that, were it not for the cutoff, there would be an infinite number of unstable modes consistent with isometry.

If μ is small, the lowest eigenvalue is bounded from below. If $\mu < \mu_{\text{cut}}$, where $\mu_{\text{cut}} = 2/3(C_0/C_1)n_{\text{max}}^{-2}$, it occurs when n coincides with the cutoff, n_{max} ; if μ is small but exceeds μ_{cut} , this minimum occurs at a value $n_0 \approx \sqrt{2/3(C_0/C_1)\mu^{-1}}$, decreasing monotonically with μ . The corresponding ground state energy grows with μ : $E_\mu \approx -4/27(C_0^3/C_1^2)\mu^{-2}$, consistent with the behavior observed in Fig. 2 for $\mu/\mu_c \ll 1$. Notice that, unlike the low-lying eigenvalues, E_μ does not increase linearly with μ in this regime.

As μ is increased further and n_0 falls through single digits, this approximation becomes increasingly unreliable. One needs to account for the non-commutativity of the operators \mathcal{H}_0 and \mathcal{H}_1 . We are particularly interested in the nodal behavior and the parity of the ground state as μ approaches criticality. This regime does not lend itself to the simple qualitative treatment presented above for small values of μ .

Intuitively, one would expect the last eigenvalue to turn positive and remain positive to be $\lambda_{\mu,1}^-$ corresponding to the eigenstate $|\lambda_{\mu,1}^- \rangle$ with a single node. Despite the unexpected erratic subcritical behavior of this state, described below, this expectation turns out to be justified.

Nodal behavior of short wavelength modes: To identify the state representing the ground

state in the neighborhood of the critical rigidity, we need to understand how long wavelength modes behave in this neighborhood. Before we do this, it is instructive to examine the behavior of short wavelength modes in a little more detail.

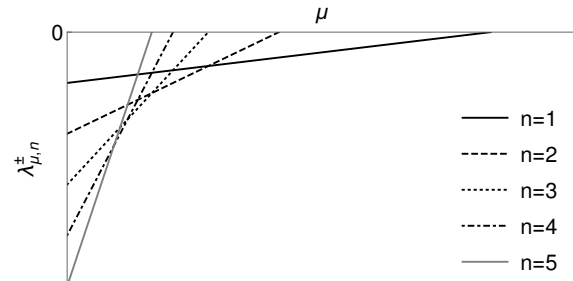


FIG. 4: $n(\mu n - 1)$ vs. μ , $n = 1, 2, 3, 4, 5$. This function captures the qualitative behavior of the spectrum of \mathcal{H}_μ when n is large. For ease of viewing, the powers of n appearing here are not those appearing in the text.

Setting constants equal to one, the eigenvalues at short wavelength behave as

$$\lambda_{\mu,n} \sim n^4(\mu n^2 - 1). \quad (25)$$

One observes the following (represented schematically in Fig. 4.):

- (i) The number of unstable modes decreases with μ . The larger n , the more unstable the mode gravitationally; but the high curvature in such modes also costs more bending energy so the sooner $\lambda_{\mu,n}$ turns positive. This occurs when $\mu_n \sim 1/n^2$.
- (ii) Eigenvalue crossovers (or degeneracies) occur at discrete values of μ . Using Eq.(25) one finds that, for each pair m and n , $\lambda_{\mu,n} = \lambda_{nm} = \lambda_{\mu,m}$ when $\mu = \mu_{nm} = (n^4 - m^4)/(n^6 - m^6)$. These crossovers occur before $\mu = \mu_n$ or μ_m . Thus the corresponding degeneracy always occurs while the eigenvalue is still negative.
- (iii) The functional dependence of the ground state energy E_μ on μ is monotonic, given by the discrete envelope bounding the spectrum from below in the manner captured in Fig. 4. Ignoring for the moment that the short wavelength expression for the eigenvalues is grossly inaccurate for small integers, we note that when $\mu > \mu_{12}$, the ground state consistent with the

spectrum described by Eq.(25) is given by the state with $n = 1$; when $\mu_{23} < \mu < \mu_{12}$ this state is replaced by the state with $n = 2$. As μ is reduced further, the ground state is provided by modes with increasing n within ever narrowing intervals of μ . At each transition, where the ground state is degenerate, E_μ suffers a kink. These are the short wavelength counterparts of the sub-critical kinks appearing in the dependence of E_μ on μ illustrated in Fig. 2. The final kinks display somewhat more complex behavior which we will describe more closely in the next subsection.

Non-Monotonicity: In longer wavelength modes, the non-commutivity of the two operators contributing to \mathcal{H}_μ cannot be ignored. Because \mathcal{H}_1 is positive and \mathcal{H}_0 negative, the eigenvalues of their sum, \mathcal{H}_μ , do not necessarily increase monotonically with μ , never mind linearly. This does not contradict the inequality Eq. (24) because \mathcal{H}_1 and \mathcal{H}_μ do not possess a simultaneous set of eigenstates. Multiple crossovers also occur. This is the origin of the striking counterintuitive non-monotonic behavior in the sub-critical regime displayed by $\lambda_{\mu,1}^-$ and $\lambda_{\mu,1}^+$ in Fig. 5. In this figure, we notice that when μ is very small, the two eigenvalues are negative, and behave monotonically as perturbation theory would predict. In this “unphysical” regime they always represent the highest energy eigenvalues, not the low energy eigenvalues we are interested in. (As we described earlier, the low energy states in this regime are represented by short-wavelength modes.) As μ is increased further, these eigenstates undergo a number of large amplitude oscillations (these are more asymmetric in the case of $\lambda_{\mu,1}^+$), briefly turning positive during these oscillations. These oscillations can be understood in terms of the sensitive dependence of the energy on μ in longer wavelength modes associated with the non-commutativity of the two competing operators. This behavior itself is not unusual: it is exhibited in two-dimensional matrix models with appropriate operators.

As μ approaches its critical value the eigenvalues again behave monotonically, signalling the domination of bending energy in these states.

These excursions, remote from the critical rigidity, would appear to imply a counterintuitive dependence of the stability on the rigidity. Fortunately, while λ_1^- is undertaking subcritical positive excursions, the corresponding state $|\lambda_1^- \rangle$ is not the ground state, a role played by some other state, not necessarily $|\lambda_1^+ \rangle$. What this state is will depend on the aspect ratio and will require a detailed numerical examination of the subcritical spectrum beyond the scope of this work.

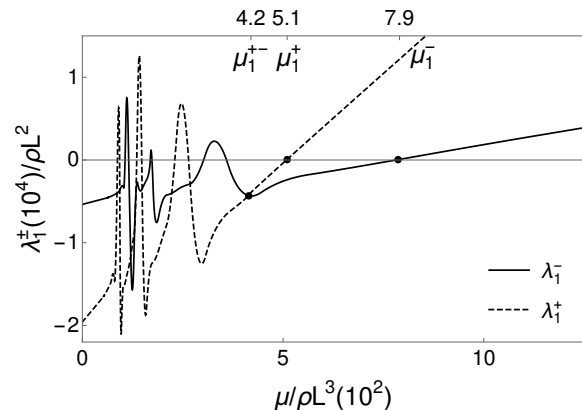


FIG. 5: $\lambda_{\mu,1}^\pm$; $H/L = 1/5$. If $\mu/\rho L \ll 1$ then $\lambda_{\mu,1}^\pm$ both grow linearly with μ , as perturbation theory predicts (in this regime, neither is the ground state); if $\mu/\rho L \gg 1$, on the other hand, $\lambda_{\mu,1}^\pm$ are again linear. The eigenvalues behave non-monotonically and exhibit multiple crossovers in the subcritical regime. The last crossover occurs at μ_1^{+-} , $\lambda_{\mu,1}^\pm$ turn positive and remain positive at μ_1^\pm . $\mu_1^- > \mu_1^+$ and is identified as the critical rigidity, μ_c . See also Fig. 2.

Low-lying eigenvalues near criticality: In general, there will exist a critical value of the rigidity, μ_n^\pm , for each mode at which the eigenvalue $\lambda_{\mu,n}^\pm$ turns positive and above which it remains so. Whereas short wavelength modes stay positive once they turn positive, as we have just seen, their misbehaved long wavelength counterparts need not remain positive. The physically significant rigidity, however, is the value where the eigenvalue turns positive for the last time. We do find that these values are ordered: $\dots < \mu_2^+ < \mu_2^- < \mu_1^+ < \mu_1^-$; the last eigenvalue to turn and stay positive is $\lambda_{\mu,1}^-$, and we identify μ_1^- as μ_c , the rigidity controlling the stability of the arch.

(i) Above μ_c , the number of nodes correlates with

energy: $0 < \lambda_{\mu,1}^- < \lambda_{\mu,1}^+ < \lambda_{\mu,2}^- < \lambda_{\mu,2}^+ < \dots$; the odd state with a single node $|\lambda_{\mu,1}^- \rangle$ is the stable ground state. There are no eigenvalue crossovers once the arch turns stable.

(ii) Within the sub-critical region, $\mu < \mu_c$, multiple eigenvalue crossovers will generally occur between long wavelength modes. However, for each pair of eigenvalues, there will be a final crossover. The last crossover to occur is between λ_1^- and λ_1^+ , occurring when $\mu = \mu_1^{+-}$. The dependence of these two eigenvalues on μ is represented in Fig. 5 for the aspect ratio $H/L = 1/5$.

We observe the following behavior in Fig. 5:

(i) If $\mu > \mu_1^{+-}$, then $\lambda_1^- < \lambda_1^+$, and $|\lambda_{\mu,1}^- \rangle$ is the ground state, albeit unstable below μ_c . If, in addition, $\mu > \mu_1^+$ (where λ_1^+ turns positive), then $|\lambda_{\mu,1}^- \rangle$ is also the unique mode of instability. If μ falls below μ_1^+ , however, $\lambda_{\mu,1}^+$ turns negative so that $|\lambda_{\mu,1}^+ \rangle$ provides an additional unstable mode. The dominant mode remains $|\lambda_{\mu,1}^- \rangle$.

(ii) As μ is lowered below the crossover value μ_1^{+-} , however, then $\lambda_{\mu,1}^+ < \lambda_{\mu,1}^-$ so that $|\lambda_{\mu,1}^+ \rangle$ replaces $|\lambda_{\mu,1}^- \rangle$ as the ground state. The parity of the dominant unstable mode changes, with an additional node. The changing parity of the dominant instability was not anticipated.

Physical representation of the near-critical unstable mode: If $\mu_1^+ < \mu < \mu_c$, we saw that the single unstable mode is $|\lambda_1^- \rangle$. This represents a symmetric buckling of a catenary, with two nodes as illustrated in Fig. 6.

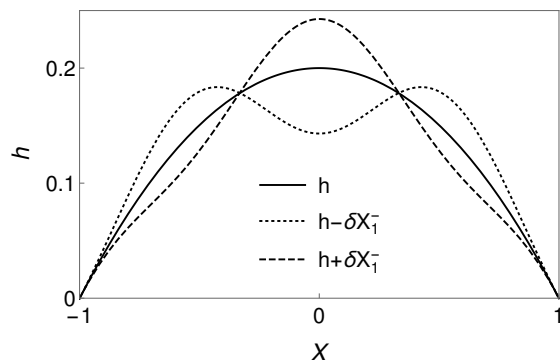


FIG. 6: Near-critical physically distinct degenerate unstable modes represented by the ground state $|\lambda_{\mu,1}^- \rangle$: $\mathbf{X} \pm \delta \mathbf{X}$. The length of the deformed curve has been increased for clarity.

The use of italics requires explanation. We know that the single tangential node in the ground state implies that the corresponding geometrical deformation has two nodes in the normal deformation. This is a straightforward consequence of the lineared isometry constraint, $\Psi' + \kappa \Phi = 0$. But this equation also implies that the nodes of Ψ never coincide with those of Φ . As a result, the catenary possesses no fixed points ($\delta \mathbf{X} \neq 0$) except at its boundaries. Note also that an initially collapsing arch must necessarily rise somewhere. It cannot fall all together at once, a consequence of the isometry constraint and the boundary conditions.

As μ is lowered further, and bending energy becomes insufficient to arrest its collapse on increasingly shorter wavelengths, the perturbed catenary will initially rise and fall an increasing number of times number of nodes, reflecting the nodal behavior of the most unstable mode, as well as the increased number of modes of instability.

Physically, each unstable mode describes two distinct geometrical modes of collapse: the spectral analysis does not distinguish energetically between the positive and negative deformations illustrated in Fig. 6. But buckling up is not the same as buckling down. To resolve this quadratic degeneracy, one needs to expand the energy out to third order in deformations, a calculation complicated by the necessity to treat the isometry constraint quadratically. Experiments with thin sheets confirm that the lower energy state is always the one falling at its center.

There are few extant higher order calculations, even without local constraints to contend with. One example we are aware of involves global rather than local constraints [45]. And, to the best of our knowledge, an independent confirmation of this result has yet to be performed.

This perturbative analysis does not discount the possibility of the subcritical arch relaxing into a new equilibrium stabilized by bending en-

ergy. Unless such a state exists, tension will build up at the antinodes as the deformation grows. This would lead to the disintegration of a masonry arch at these *hinges* and the subsequent free fall of the fragments.

VI. CONCLUSIONS AND FUTURE WORK

In this paper, we have introduced a geometrical framework to assess the stability of a free-standing thin-walled structure. This involves understanding how surfaces deform isometrically, the identification of the appropriate bending energy and the spectral analysis of the self-adjoint operator controlling perturbations about equilibrium. While geometry was well-known to play a role in our identification of equilibrium its role in understanding the behavior of deformations about equilibrium does not appear to have been appreciated, never mind explored in this limit. In general there is, of course, a lot more to solid mechanics than is captured by our phenomenological model [46]. One should think of this energy as a phenomenological one, where the emphasis is on capturing the essential features of the problem. While deriving the appropriate bending energy from first principles is likely to be no simple matter, when the dust settles one would expect it to look not unlike the energy written down in Eq.(5), with spontaneous curvatures determined—consistent with the protocol—by the equilibrium reference values of the curvature. If, however, the thin wall approximation does not apply, our geometrical approach is rendered invalid and it is necessary to approach the subject very differently.

We have illustrated this framework using the historically significant example of a catenary arch. The example itself may appear quaint; its analysis does, however, illustrate the extraordinarily sensitive dependence of the stability on the rigidity.

It should be stressed that we have not attempted to capture every feature of the linear stability of a catenary arch much less attempt to examine any more complicated geometry. Understanding the complex erratic behavior of the

spectrum of the self-adjoint operator controlling the response, alone, would keep us occupied for a while. We have, however, described a number of the essential elements of the problem, justifying not just why the Hookean construction works—something every mason knows—but also providing a framework to predict if an arch will stand and how it fails if it does not. We hope our work will inspire others to pursue these issues.

The natural next step is to examine the stability of genuine three-dimensional structures. Indeed, a complete treatment of the catenary vault should rightly accommodate deformations that break the cylindrical symmetry, deforming the arch into a more general metrically flat tangent developable surface [44] consistent with the boundary conditions. As it turns out, when the rigidity is isotropic as we have supposed for simplicity, such modes of failure never form the ground state so treating them does not change our conclusions. If, however, the wall is constructed using an anisotropic material, so that H_B in Eq.(5) is replaced by something like

$$H_B = \frac{1}{2} \sum_I \mu_I \int dA (C_I - C_I(u))^2, \quad (26)$$

with different moduli along orthogonal directions, the dominant mode of instability would be expected to lie along the transverse direction if bending is soft along this direction, or equivalently, μ_2/μ_1 is sufficiently small.

In general, the stability of a three-dimensional structure will depend very sensitively both on its Gaussian curvature as well as the boundary conditions. A mathematical surface with positive Gaussian curvature, such as a closed dome on a fixed base, does not support any small isometric deformations [2]. So if stretching is not accommodated, one would expect isometry alone to stabilize the structure. This may be true of pingpong balls. The fault with this reasoning here is that vertical cracks will develop towards the base of a masonry dome where the structure becomes subject to substantial tension (or hoop stresses) along the parallels. The two sides of the crack will behave as free boundaries that become free to move independently under deformation. The stability of the dome

needs to be reassessed accommodating the free boundaries along these cracks. It is a sobering thought that a reliable geometrical framework to accommodate free boundaries on thin walls remains to be developed. But that is another story.

Acknowledgments: We benefitted from dis-

cussions with L Mahadevan during the early stages of this work. Indeed, it was he who pointed out that the stability of masonry was a question that was due reappraisal in the thin wall limit. We also thank James Hanna, Martin Müller and David Steigmann for useful comments. This work was supported in part by CONACyT grant no. 180901 to JG.

-
- [1] J. Heyman *The Stone Skeleton: Structural Engineering of Masonry Architecture* (Cambridge University Press, 1995)
- [2] M. Spivak *A Comprehensive Introduction to Differential Geometry* Vol. 5 (Publish or Perish, 1975) Note to the wary reader: despite appearances one does not need to wade through the first four volumes to benefit from a reading of the relevant chapter.
- [3] A.V. Pogorelov *Bendings of surfaces and stability of shells* Vol. 72. (American Mathematical Soc., 1988)
- [4] R. Harnach and H. Rothert *International Journal of Solids and Structures* **12** 359 (1976)
- [5] B. Audoly and Y. Pomeau *Elasticity and geometry: from hair curls to the non-linear response of shells* (OUP Oxford, 2010)
- [6] S. Verpoort *The geometry of the second fundamental form: curvature properties and variational aspects* (Thesis Leuven, 2008)
- [7] For a review see T. Witten *Rev. of Mod. Phys.* **79** 643 (2007);
- [8] E. Cerda, L. Mahadevan and J.M.Pasini *PNAS* **101** 1806 (2004); E Cerda and L Mahadevan *Elastica Proc. R. Soc. A* **461** 671 (2005);
- [9] Y. Klein, E. Efrati, and E. Sharon *Science* **315** 1116 (2007);
- [10] A. P. Korte, E. L. Starostin, and G. H. M. van der Heijden *Proc. Roy. Soc. London A* **467** 285 (2011);
- [11] J. Gemmer and S. C. Venkataramani *Soft Matter* **9** 8151 (2013)
- [12] Y.-C. Chen, R. Fosdick, E. Fried *Journal of Elasticity* (in press). (doi:10.1007/s10659-017-9637-2)
- [13] Consult the Wikipedia entry for *Taq Kasra*. This archway, constructed sometime after 540 CE, is essentially all that remains of the city of Ctesiphon, located in what is currently Iraq. Constructed without centring, it remains the largest vault of unreinforced brickwork ever constructed.
- [14] See, for example, P. Block, M. DeJong and J. Ochsendorf *Nexus Network Journal* **8** 13 (2006)
- [15] An informal discussion is provided in <http://civil.lindahall.org/design.shtml>
For those readers interested in the anagram itself, see <https://newtonexcelbach.wordpress.com/2010/07/14/arches-anagrams-and-plagiarism/>
- [16] The year before his death, the geometer Robert Osserman wrote a thoughtful essay on the catenary arch. See R. Osserman *Mathematics of the gateway arch* in Notices of the American Mathematical Society **57** 220-229 (2010)
- [17] In a semi-circular Roman arch, the wayward thrust is tamed by the weight distributed above it.
- [18] J. Guven and M.M. Müller, *J. Phys. A: Math. and Gen.* **41** 055203 (2008)
- [19] E. Vouga, M. Höbinger, J. Wallner, and H. Pottmann. *Design of self-supporting surfaces* ACM Trans. Graphics, **31** 1 (2012)
- [20] S. Adriaenssens (Ed), P. Block (Ed.), D. Veenendaal (Ed.), C. Williams (Ed.) *Shell Structures for Architecture: Form Finding and Optimization* (Routledge, 2014)
- [21] Unfortunately, building temples in stone can still be slow. Gaudi's Sagrada Familia, begun in 1882, is only nearing completion at the time of writing. *Sagrada Família enters final construction phase* Guardian 27 October 2015
<http://www.theguardian.com/artanddesign/antoni-gaudi>
- [22] P. Jodidio *Zaha Hadid* (Taschen, 2016)
- [23] Our focus is on the role of bending energy in arresting the collapse of an otherwise gravitationally unstable configuration. We do not examine its stability under the displacement of its support.
- [24] J. Heyman, *Equilibrium of shell structures* (Clarendon Press Oxford, 1977)
- [25] M. Levy and M. Salvadori *Why Buildings Fall Down: How Structures Fail* (W. W. Norton & Company 2002)
- [26] Foster and Partners' Mexico City Airport
<https://vimeo.com/105157027> min 5:50
- [27] New international airport for Mexico City
https://en.wikipedia.org/wiki/Planned_Mexico_City_international_airport
- [28] L. Landau and E. Lifshitz *Theory of Elasticity* (Pergamon Press, 1959)
- [29] Lord Rayleigh *On bells* The London, Edinburgh, and Dublin Philosophical Magazine and Journal of Science, **29**(176), January 1890
- [30] W. Helfrich *Z. Naturforsch. C* **28** 693 (1973).
- [31] U. Seifert *Advances in Physics* **46** 13 (1997)
- [32] S. Svetina and B. Žekš, *Eur. Biophys. J.* **17**, 101 (1989)
- [33] J Guven, G Huber, and D M Valencia *Phys. Rev. Lett.* **113** 188101 (2014)
- [34] J.R. Frank and M. Kardar *Phys. Rev. E* **77** 041705 (2008)
- [35] N. Walani, J. Torres, A. Agrawal *Phys. Rev. E* **89** 062715 (2014)
- [36] M.A. Dias, J.A. Hanna, C.D. Santangelo *Phys. Rev. E* **84** 036603 (2011)
- [37] No analogue exists for a pure fluid membrane.
- [38] R. Capovilla, J. Guven and J. A. Santiago *Journal of Physics A: Mathematical and General* **36** 23 (2003)
- [39] R. Capovilla and J. Guven, *J. Phys. A: Math. and Gen.*

35 6233 (2002)

- [40] A. Gray *A Modern Differential Geometry of Curves and Surfaces with Mathematica* (Chapman & Hall/CRC 2006)
- [41] J. Guven, M.M. Müller and Pablo Vzquez-Montejo *Journal of Physics A: Mathematical and Theoretical* **45** 1 (2011)
- [42] $\langle \Psi_1 | \Psi_2 \rangle = \int ds \Psi_1(s) \Psi_2(s)$.
- [43] We choose as our basis (expressed as functions of X rather than s) the functions which result from the Gram-Schmidt orthogonalization of the following sums of Fourier modes:

$$f_n^+(X) = \frac{1}{\sqrt{L}} \left(\cos \frac{(2n+1)\pi X}{2L} + \frac{2n+1}{2n+3} \cos \frac{(2n+3)\pi X}{2L} \right),$$

and

$$f_n^-(X) = \frac{1}{\sqrt{L}} \left(\sin \frac{n\pi x}{L} + \frac{n}{n+1} \sin \frac{(n+1)\pi X}{L} \right).$$

These modes are consistent with the boundary conditions: $f_n, f_n', f_n'' = 0$ on $X = \pm L$.

- [44] M. Do Carmo *Differential Geometry of Curves and Surfaces* (Prentice hall 1976)
- [45] O.Y. Zhong-Can and W. Helfrich *Phys. Rev. Lett.* **59** 2486 (1989)
- [46] D. Steigmann *Archive for Rational Mechanics and Analysis* **150** 127 (1999)